Available online at www.sciencedirect.com
ScienceDirect
Catalysis Today 126 (2007) 441–448
CATALYSIS TODAY
www.elsevier.com/locate/cattod

Effects of ZrO_2/Al_2O_3 properties on the catalytic activity of Pd catalysts for methane combustion and CO oxidation

Yun Guo [a,*], Guanzhong Lu [a], Zhigang Zhang [a], Liangzhu Jiang [a], Xiaohong Wang [a], Shuben Li [b], Bing Zhang [b], Jianzhong Niu [b]

[a] *Lab for Advanced Materials, Research Institute of Industrial Catalysis, East China University of Science and Technology, Shanghai 200237, PR China*

[b] *State Key Laboratory of Oxo Synthesis and Selective Oxidation, Lanzhou Institute of Chemical Physics, Chinese Academy of Sciences, Lanzhou 73000, PR China*

Available online 20 July 2007

Abstract

Zirconia supported on alumina was prepared and characterized by BET surface area, X-ray diffraction (XRD), X-ray photoelectron spectra (XPS), temperature programmed desorption (TPD), and pulse reaction. 0.2% $Pd/ZrO_2/Al_2O_3$ catalyst were prepared by incipient wetness impregnation of supports with aqueous solution of $Pd(NO_3)_2$. The effects of support properties on catalytic activity for methane combustion and CO oxidation were investigated. The results show that ZrO_2 is highly dispersed on the surface of Al_2O_3 up to 10 wt.% ZrO_2, beyond this value tetragonal ZrO_2 is formed. The presence of a small amount of ZrO_2 can increase the surface area, pore volume and acidity of support. CO–TPD results show that the increase of CO adsorption capacity and the activation of C=O bond after the presence of ZrO_2 lead to the increase of catalytic activity of Pd catalyst for CO oxidation. CO pulse reaction results indicate that the lattice oxygen of support can be activated at lower temperature following the presence of ZrO_2, but it does not accelerate the activity of 0.2% $Pd/ZrO_2/Al_2O_3$ for methane combustion. 0.2% $Pd/ZrO_2/Al_2O_3$ dried at 120 °C shows highest activity for CH_4 combustion, and the activity can be further enhanced following the repeat run. The increase of treatment temperature and pre-reduction can decrease the activity of catalyst for CH_4 combustion.

Keywords: ZrO_2/Al_2O_3; Pd catalyst; CH_4 combustion; CO oxidation; TPD; Pulse reaction

1. Introduction

The catalytic combustion of methane and CO oxidation have drawn a great attention in recent decades because of the interests arising from power generation and pollution abatement. Methane is a well-known greenhouse gas and its strong C–H bonds are most difficult to be broken. For the catalytic combustion of methane and CO oxidation, the supported Pd catalyst is one of the most active catalysts [1,2]. Many studies show that the catalytic performance of Pd/Al_2O_3 is influenced greatly by the Pd loading, Pd crystallite morphology, pretreatment condition, reaction condition, and so on. Although the catalytic combustion of methane and CO oxidation over Pd catalyst using alumina as support has been extensively investigated, other materials as the support of Pd catalyst have been tested as well [3–8]. For example, Epling and Hoflund [9] demonstrated that Pd/ZrO_2 catalyst shows high activity and achieves complete conversion of methane at temperature under 300 °C.

The effects of Pd loading, Pd dispersion, phase structure and precalcination of ZrO_2, methane-to-oxygen ratio, coexistence of water vapor on the performance of Pd/ZrO_2, and its decay have been studied [9–13]. However, the catalytic oxidation mechanism and active surface species for the catalytic combustion of methane have not been completely identified due to the difficulties of surface characterization of catalyst under reaction condition. Yang et al. [14] have investigated the nature of the surface sites over Pd/ZrO_2 and Pd/Al_2O_3 using CO chemisorption. Ciuparu et al. [15] used the pulse reaction of the isotopically labeled reaction mixture to investigate the contribution of the lattice oxygen in the methane catalytic combustion reaction. Fujimoto et al. [10] studied the effects of

* Corresponding author. Fax: +86-21-64253703.
E-mail address: yunguo@ecust.edu.cn (Y. Guo).

0920-5861/$ – see front matter © 2007 Elsevier B.V. All rights reserved.
doi:10.1016/j.cattod.2007.06.015

Pd dispersion and oxidation–reduction treatments on the catalytic activity of Pd/ZrO_2 for the methane combustion. Grunwaldt et al. [16] used *in situ* EXAFS to explore the oxidation state and structure of Pd/ZrO_2.

Although ZrO_2 with a large surface area can be prepared, its relative lower surface area compared with alumina and higher cost limit the generous use of ZrO_2. ZrO_2 dispersed on high surface area support may solve these problems because combining the unique properties of ZrO_2 and high surface area of supports can be achieved. Souza and Schmal [17] demonstrated that $Pt/ZrO_2/Al_2O_3$ were most active and stable for autothermal reforming of methane among Pt/ZrO_2, Pt/Al_2O_3, and $Pt/ZrO_2/Al_2O_3$. Some studies of preparation method and surface properties of ZrO_2 supported on large surface area supports (such as Al_2O_3 and SiO_2) have been reported [18–20]. These works mainly concentrated on the effect of preparation method on the dispersion state of ZrO_2, the interaction between ZrO_2 and support, the surface acidity and so on.

In this paper, the physicochemical properties of ZrO_2/Al_2O_3 were studied, and the effects of support properties on the catalytic activity of supported Pd catalyst for the methane combustion and CO oxidation were investigated.

2. Experimental

2.1. Preparation of sample

γ-Al_2O_3 (20–40 mesh) was calcined at 750 °C for 3 h before the introduction of ZrO_2. ZrO_2/Al_2O_3 composite supports were prepared by impregnating Al_2O_3 with the $ZrO(NO_3)_2$ aqueous solution. The mixture was stirred, and then the water was removed under reduced pressure at about 65 °C. The supports were dried at 120 °C and calcined in air at 500 °C for 6 h (or at 700 °C for 5 h). The ZrO_2 content was in the range of 2–20 wt%. ZrO_2/Al_2O_3 composites were calcined at 500 °C for 6 h unless a special annotation was given.

The supported Pd catalysts were prepared by incipient wetness impregnation of supports with aqueous solution of $Pd(NO_3)_2$. The samples impregnated were dried at 120 °C for 10 h to get the catalysts signed as CN-1. The CN-1 catalysts were calcined in air at 500 °C for 3 h to get CN-2 catalysts. CN-2 catalysts were reduced in H_2 at 400 °C for 3 h to get CN-3 catalysts. The loading of Pd was about 0.2 wt%.

2.2. Characterization of sample

The BET surface areas of supports were measured by a Micromeritics ASAP 2010 Sorptometer using nitrogen as adsorption gas. X-ray diffraction (XRD) patterns were recorded on a D/MAXRB 12KWX powder diffractometer with Cu Kα radiation. The X-ray photoelectron spectra (XPS) were obtained with a VG ESCALAB 210 spectrometer with Mg Kα radiation, operating at 10 kV and 20 mA. The binding energy of adventitious C_{1s} (284.6 eV) was used as a reference. The FT-IR spectra of samples were recorded on a Nicolet Nexus 670 FT-IR spectrometer, and the samples to be measured were ground with KBr and pressed into thin wafers.

2.3. Temperature–programmed desorption (TPD) and pulse reaction

TPD and pulse reaction were performed with a commercial temperature-programming system (Altamira Instruments, AMI-100). The chemical components of TPD and pulse reaction were monitored by an on-line quadrupole mass spectrometer (Ametek Instruments, Dycor 1000), and the multiple mass peaks could be recorded simultaneously during experiments.

In the TPD measurement, the sample was first calcined at 500 °C in He (20 cm^3/min) for 20 min, and then cooled to the adsorption temperature. After the adsorption gas (15 cm^3/min) passed through 500 mg sample for 20 min to get saturated adsorption, the catalyst bed was flushed with He for 10 min. TPD was performed by heating the sample in He (20 cm^3/min) at a rate of 20 °C/min. 4.9% NH_3/He and 5% CO/Ar were used in NH_3–TPD and CO–TPD, respectively. The blank experiment was carried out with same procedure except the adsorption of NH_3 or CO.

In the pulse reaction experiment, 500 mg sample was pretreated by the procedure above, and then the pulse reaction of CO was performed at different temperature. The composition of reaction gas was 5% CO/Ar.

2.4. Catalytic activity test

The activities of catalysts for the methane combustion and CO oxidation were evaluated in a fixed-bed reactor at atmospheric pressure. The reaction gas of 1% CH_4/air or 4% CO/air was fed to the catalyst bed at a space velocity of 10,000 h^{-1}. The reaction temperature was programmed at room temperature to the temperature of CH_4/CO complete conversion at a rate of 4 °C/min. The conversion of CH_4 or CO was analyzed at 10 or 5 °C intervals by an on-line gas chromatography. Blank experiments were performed filling the reactor with quartz wool only.

3. Results and discussion

3.1. XRD

The XRD patterns of alumina and ZrO_2/Al_2O_3 are shown in Fig. 1. The diffraction pattern of sample with lower ZrO_2 content (<10 wt%) is similar to that of Al_2O_3. However, the weak diffraction peaks of crystallized ZrO_2 can be observed on 10% ZrO_2–Al_2O_3. The intensities of diffraction peaks increase with increasing ZrO_2 content. For 20% ZrO_2/Al_2O_3, three characteristic peaks of tetragonal ZrO_2 were observed at about 30, 50 and 60°, respectively. The results above show that ZrO_2 is highly dispersed on the surface of Al_2O_3 when ZrO_2 content is lower than 10wt%; tetragonal ZrO_2 particles have formed when ZrO_2 content is >10 wt%. Increasing the calcination temperature to 700 °C, the intensities of characteristic peaks of

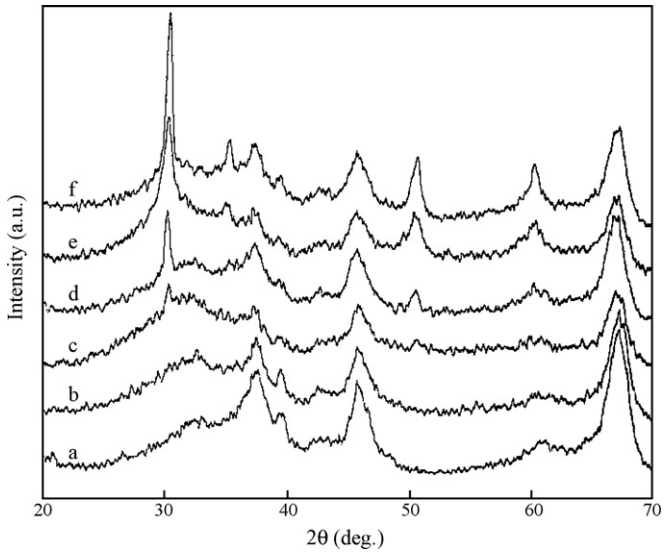

Fig. 1. XRD patterns of alumina (a) and ZrO_2/Al_2O_3 with ZrO_2 content of 5% (b), 10% (c and e) and 20% (d and f). (a–d was calcined at 500 °C for 6 h, e and f was calcined at 700 °C for 5 h).

tetragonal ZrO_2 increase significantly, which implying the higher crystalloid degree of ZrO_2.

3.2. Textural properties

The BET surface areas and pore properties of ZrO_2/Al_2O_3 calcined at 500 °C for 6 h are summarized in Table 1. The ZrO_2/Al_2O_3 composite oxides with low ZrO_2 content show larger surface areas and larger pore volumes than pure Al_2O_3, e.g. 2 wt% ZrO_2–Al_2O_3 has the highest surface area. The surface area decreases gradually with continuously increasing ZrO_2 content.

In the process of preparing the ZrO_2/Al_2O_3, we observed that the pH value change of the acidic $ZrO(NO_3)_2$ impregnation solution after immersing Al_2O_3 in it, such as the pH value increased from 2.1 to 3.9 in preparing 2% ZrO_2/Al_2O_3. The strong acidic solution can erode the surface of Al_2O_3 and break Al–O–Al bond among the particles of Al_2O_3. The insertion of Zr^{4+} blocks the formation of Al–O–Al bond again after drying and calcination, which may promote the formation of new pores and the decrease of the particle size and crystallization degree of Al_2O_3. The XRD results in Fig. 1 show that the intensities of diffraction peaks of Al_2O_3 decrease following the presence of ZrO_2, that is to say, the crystallization degree of Al_2O_3 has declined. In the preparation of the ZrO_2/Al_2O_3 supports with high ZrO_2 content, the acidity of $ZrO(NO_3)_2$ impregnation solution increased with increasing $ZrO(NO_3)_2$ content, such as, the pH values of impregnating solutions were 2.3 and 1.4 after impregnation for 10% and 20% ZrO_2/Al_2O_3. When the acidity of the solution increases to a certain extent ($pH \leq 3$), it can cause the solubility and re-deposition of Al_2O_3, which results in the decrease of the surface areas of sample [21]. The blocking of some pores of Al_2O_3 by ZrO_2 crystallites can cause the decrease of surface area too.

Table 1
BET surfaces area and pore properties of ZrO_2/Al_2O_3 calcined at 500 °C for 6 h

Sample	Surface area (m^2/g)	Pore volume (cm^3/g)	Average pore diameter (nm)
Al_2O_3	138	0.43	10.7
2% ZrO_2/Al_2O_3	147	0.48	11.2
5% ZrO_2/Al_2O_3	146	0.48	11.3
10% ZrO_2/Al_2O_3	135	0.42	10.7
20% ZrO_2/Al_2O_3	129	0.31	8.5

Table 2
Binding energy of Al_2O_3 and ZrO_2/Al_2O_3 calcined at 500 °C for 6 h

ZrO_2 (wt%)	Binding energy (eV)	
	Al 2p	Zr $3d_{5/2}$
0	74.5	–
5	74.6	182.4
10	74.5	182.2
20	74.6	182.2

3.3. XPS

The binding energies of Al 2p and Zr 3d are summarized in Table 2. The Zr $3d_{5/2}$ binding energy decreased slightly with increasing ZrO_2 content. The binding energy (182.2 eV) of Zr $3d_{5/2}$ in 20% ZrO_2/Al_2O_3 agrees with binding energy of Zr^{4+} in pure ZrO_2 [20]. The slight increase in the binding energy of $Zr3d_{5/2}$ for the samples with lower ZrO_2 content may be due to a change in the coordination number of zirconium. Damyanova et al. [20] attributed this phenomenon to the interaction of Zr with Al atom and formation of Zr–O–Al bond.

3.4. NH_3–TPD

The amount of NH_3 adsorbed can be used to measure the number of total acid sites including Lewis acid sites and Bronsted acid sites. The NH_3–TPD profiles of Al_2O_3 and ZrO_2/Al_2O_3 are shown in Fig. 2, and the amount of NH_3 desorbed is listed in Table 3.

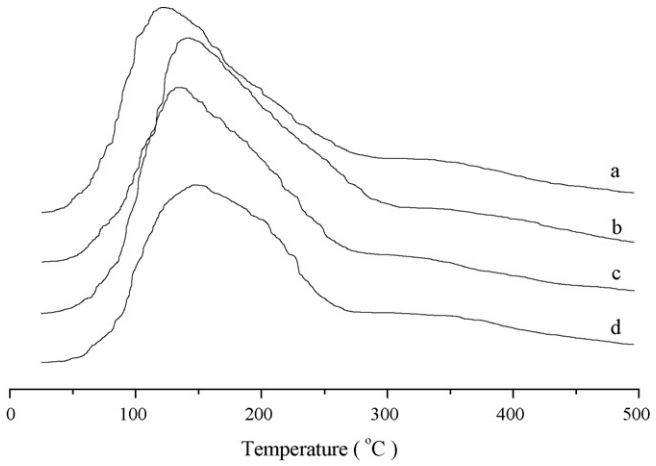

Fig. 2. NH_3–TPD profiles of Al_2O_3 (a) and ZrO_2/Al_2O_3 with ZrO_2 content of 5% (b), 10% (c) and 20% (d).

Table 3
Desorbed quantity of CO_2 and NH_3 during TPD over Al_2O_3 and ZrO_2/Al_2O_3 calcined at 500 °C for 6 h

Sample	Amount of NH_3 desorbed (mmol/m^2 of oxide)	Amount of CO_2 desorbed (μmol/g of oxide)		
		Peak 1	Peak 2	Sum
Al_2O_3	0.086	–	11.70	11.70
5% ZrO_2–Al_2O_3	0.089	0.70	12.59	13.29
10% ZrO_2–Al_2O_3	0.095	1.77	17.29	19.06
20% ZrO_2–Al_2O_3	0.083	2.89	17.83	20.72

The desorption peaks of NH_3 shifted to higher temperature after the introduction of ZrO_2 into alumina, which indicated that the ZrO_2/Al_2O_3 had higher acidity strength than pure Al_2O_3. The concentration of acid sites increases with increasing ZrO_2 content up to 10% and decreases with continuously increasing ZrO_2 content. Combining with XPS data, the increase of acid sites concentration is probably due to the interaction between ZrO_2 and Al_2O_3.

3.5. CO–TPD

CO–TPD of Al_2O_3 and ZrO_2/Al_2O_3 were performed, and the results are shown in Fig. 3. The significant mass peak of CO_2(44) was observed over Al_2O_3 at the temperature range 300–500 °C. The peaks of CO(28) and O(16) can be detected at the same position (Fig. 3a). For CO–TPD of ZrO_2/Al_2O_3, two peaks of CO_2 were detected. The strong CO_2 peak shifted to lower temperature (200–300 °C), and a new weak peak was located at about 100 °C (Fig. 3 b–d).

Based on the standard mass spectra of CO_2, peaks of CO(28) and O(16) were produced by dissociation of CO_2 in the mass spectrometer. It indicated that CO adsorbed on support desorbed in the form of CO_2 during the process of TPD. For the CO_2 peak at lower temperature on the ZrO_2/Al_2O_3, no peaks of CO and O were observed at the position of CO_2 peak for the ZrO_2/Al_2O_3 samples (<20% ZrO_2), which was due to the fact that the quantity of CO_2 was so little that the peaks of 28 and 16 produced could not be detected.

In general, CO_2 formation has the following routes: (1) CO disproportionation; (2) adsorbed CO reacting with oxygen in He stream; (3) water gas shift reaction; (4) decomposition of CO_3^{2-} species on the surface. In the blank experiments, CO_2 and H_2O were not detected before 500 °C, so the last two routes can be excluded. Based on the purity of He flow (He ≥ 99.999%) and the time of desorption, it could be concluded that CO_2 was formed via CO disproportionation and desorbed from the surface because of its weaker bonding with the surface. In order to confirm the view above, the O_2 pulse reactions were performed at the end of CO–TPD. The CO_2(44) peak can be observed following the O_2 pulse. In the blank experiments, CO_2 cannot be detected after O_2 pulse over Al_2O_3 and ZrO_2/Al_2O_3. The results of O_2 pulse reaction proved the existence of C deposition formed by CO disproportionation reaction on the surface of samples.

The adsorption capacity of CO on the samples can be calculated from the amount of CO_2 desorbed, the results are listed in Table 3. It shows that CO adsorption capacity increases with an increase of the ZrO_2 content. Shift of the CO_2 desorption peak to low temperature and the presence of a new desoption peak of CO_2 at about 100 °C show that the presence of ZrO_2 can activate the bond of C=O and accelerate the disproportionation reaction of CO adsorbed.

3.6. CO pulse reaction

The results of CO pulse reaction on Al_2O_3 and ZrO_2/Al_2O_3 at different temperature are shown in Figs. 4–6. For CO pulse reaction at room temperature, the CO peak lagged behind the

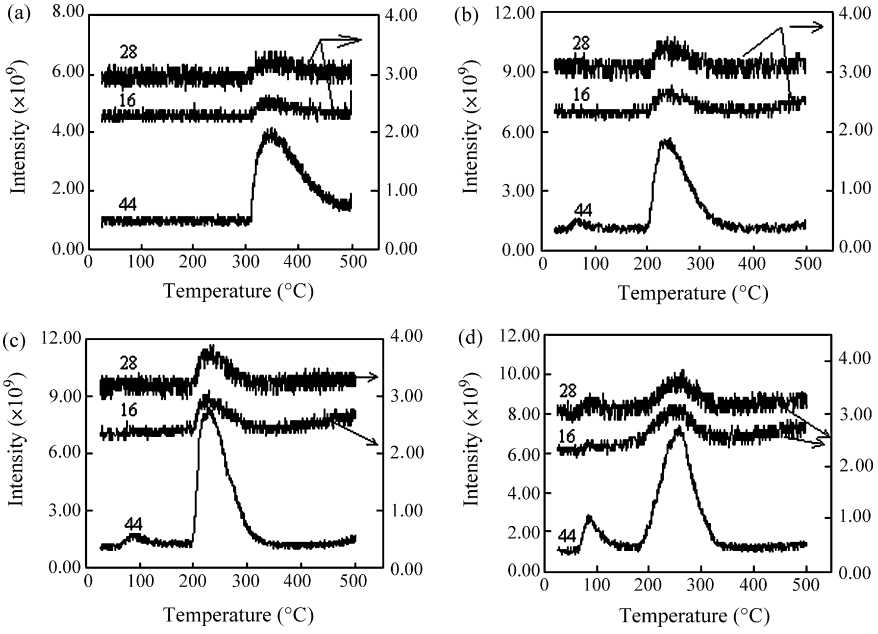

Fig. 3. CO–TPD spectra of Al_2O_3 (a), 5% ZrO_2/Al_2O_3 (b), 10% ZrO_2/Al_2O_3 (c) and 20% ZrO_2/Al_2O_3 (d).

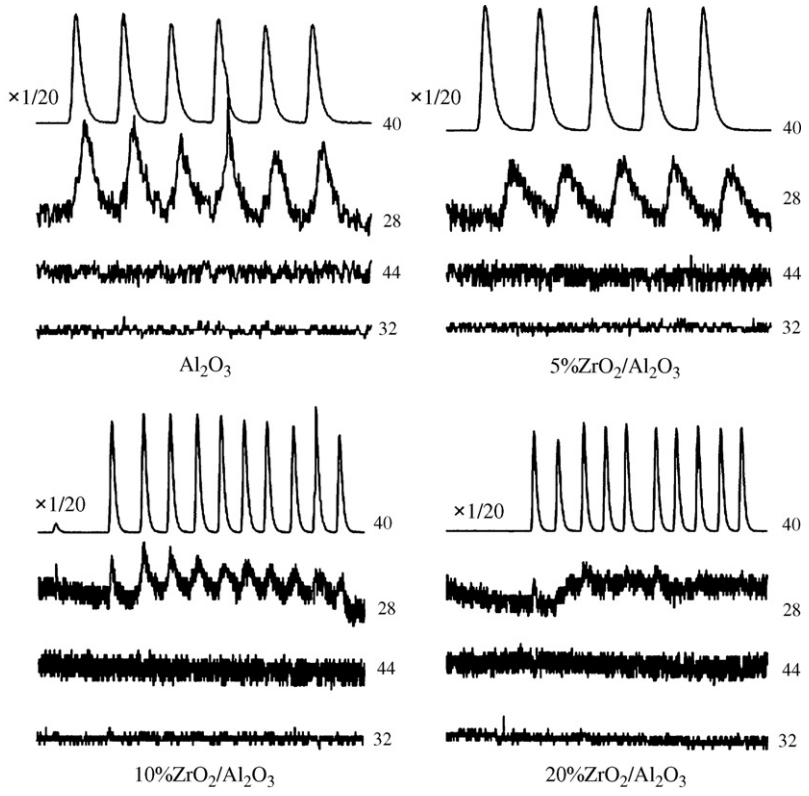

Fig. 4. CO pulse reaction over Al_2O_3 and ZrO_2/Al_2O_3 at room temperature.

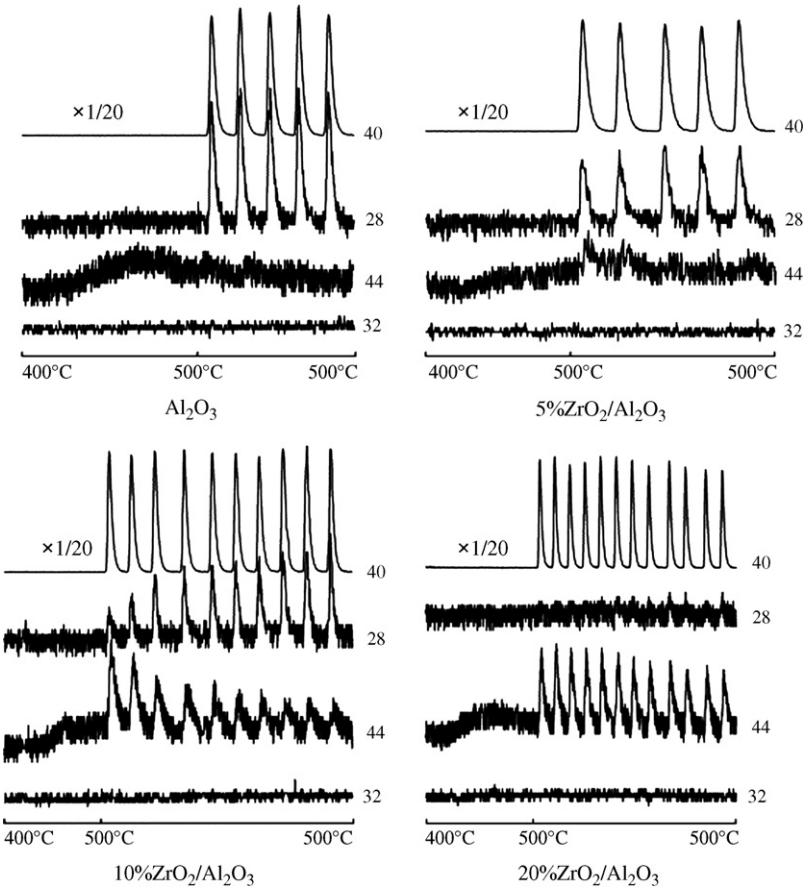

Fig. 5. CO pulse reaction over Al_2O_3 and ZrO_2/Al_2O_3 at 500 °C.

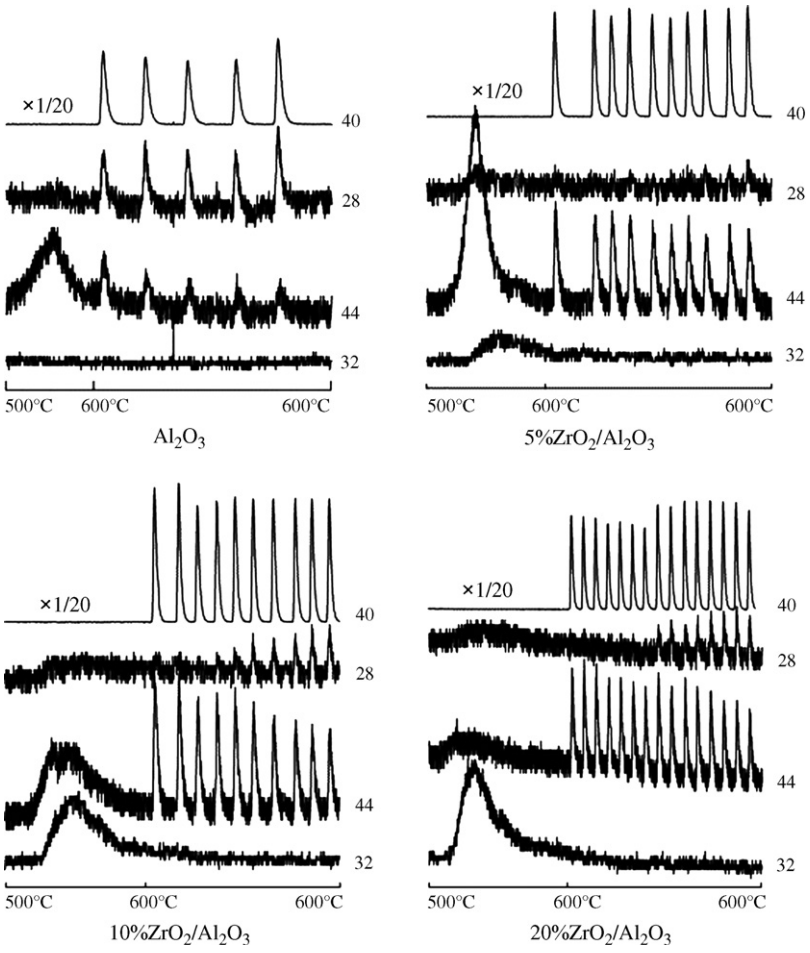

Fig. 6. CO pulse reaction over Al_2O_3 and ZrO_2/Al_2O_3 at 600 °C.

peak of Ar(40) (Fig. 4), which indicated that CO could adsorb on the surface of sample. The adsorption capacity of CO increased with increasing ZrO_2 content, such as CO also adsorbed nearly completely on 20% ZrO_2–Al_2O_3 in 10 pulses, which was consistent with the results of CO–TPD.

In the process of elevating the temperature, the desorption of CO was not observed. When the temperature reached 500 °C, CO_2 appeared following the CO pulse on all the samples except Al_2O_3 (Fig. 5). The abilities of samples for oxidizing CO increase with increasing ZrO_2 content. Only a little CO_2 was found in the pulse reaction on 5% ZrO_2/Al_2O_3. For 20% ZrO_2/Al_2O_3, CO was nearly completely converted to CO_2 in 10 pulses.

The adsorbed oxygen on the surface is first activated in the process of elevating temperature, but it is consumed quickly due to a limited amount. Although the lattice oxygen is difficult to be activated, the surface lattice oxygen can get compensation from bulk phase continuously. So, the role of lattice oxygen can make catalyst sustain oxidation ability for a certain period of time in the absence of oxygen.

Based on the results of CO pulse reaction at 500 °C, the formation of CO_2 on the 5% ZrO_2/Al_2O_3 was assigned mainly to the function of surface adsorbed oxygen, which consumed so quickly that no CO_2 could be detected after 5 pulses. For 20% ZrO_2/Al_2O_3, the lattice oxygen played the major role in the pulse reaction, and CO was nearly completely oxidized to CO_2 in 10 pulses. The cooperation of lattice oxygen and surface adsorbed oxygen caused the intensities of CO_2 peaks decreased gradually on 10% ZrO_2/Al_2O_3, and still can be detected clearly after 10 pulses. The results above show that the ability of sample providing active oxygen species increases and the temperature of lattice oxygen activated decrease with an increase of ZrO_2 content.

ZrO_2 is a well-known oxygen supplier, and its oxygen mobility is about three times higher than that of Al_2O_3 [22]. The oxygen vacancies on the surface of ZrO_2 can be created by extraction of lattice oxygen ions during the reaction [23–25], and get replenishment through the diffusion of lattice oxygen from bulk phase. The number and diffusion of oxygen vacancies in ZrO_2 can be increased significantly by doping with lower valance metal ions, such as Y^{3+} [26]. For ZrO_2–Al_2O_3, the change of coordination environment due to the interaction between ZrO_2 and Al_2O_3 results in increasing the number of oxygen vacancies and the diffusion of lattice oxygen.

The desorption of O_2(32) can be observed on ZrO_2/Al_2O_3 at the temperature range 500–600 °C, and the desorption amount of O_2 increased with increasing ZrO_2 content (Fig. 6). For pulse reaction at 600 °C, CO_2 can be detected on all the samples following CO pulse (Fig. 6). The intensity of CO_2 peak decreased significantly with increasing the pulse number on

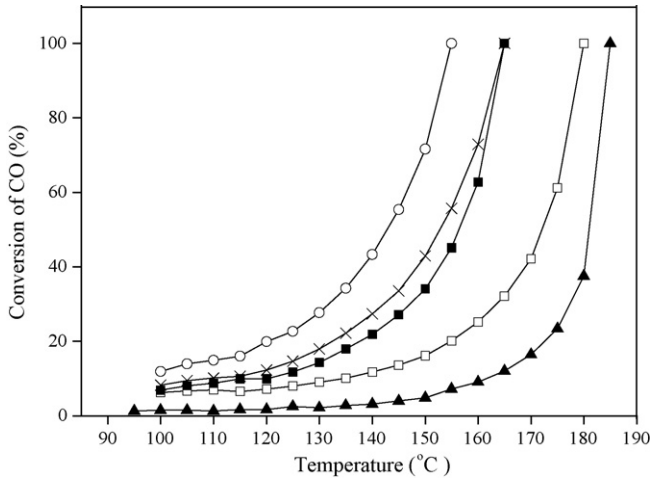

Fig. 7. CO oxidation activity of CN-3 catalysts supported on: (▲)Al_2O_3; (□)2% ZrO_2–Al_2O_3; (■)5% ZrO_2/Al_2O_3; (×)10% ZrO_2/Al_2O_3; (○)20% ZrO_2/Al_2O_3.

Al_2O_3, and only a little CO can be found on the 5% ZrO_2/Al_2O_3 after 10 pulses. However, the more significant CO peaks can be observed after several pluses on 20% ZrO_2/Al_2O_3 at 600 °C. It is suggested that the sample cannot provide enough active oxygen species to oxidize CO due to desorption of lattice oxygen.

3.7. Catalytic activity

3.7.1. CO oxidation

Fig. 7 shows the CO oxidation over CN-3 catalysts. The reactor packed only quartz fiber was inactive for the CO oxidation under reaction condition. All catalysts using ZrO_2/Al_2O_3 as the support showed higher activity than Pd/Al_2O_3 and their activities increased with increasing ZrO_2 content. Combining with Fig. 3 and Table 3, it can be drawn that the presence of ZrO_2 is helpful for the chemical adsorption of CO and activation of C=O bond on the catalysts, and obviously promote the performance of Pd/Al_2O_3 catalyst for the CO oxidation reaction.

3.7.2. Methane combustion

The catalytic activities of different catalysts for methane combustion are summarized in Tables 4–6, respectively. The results show that the treatment conditions can influence the activity of catalysts for CH_4 combustion significantly. Among the catalysts, CN-1 catalysts show the highest activities for CH_4 combustion, and behave a slight higher activity in the second run. Baldwin and Burch [27] have reported that the catalyst activity increases as a function time, and their Pd/Al_2O_3 catalyst becomes four times more active over a 300-h time period. The enhanced activity of CN-1 catalyst in the second run was possibly induced by the formation and optimization of active phase in the reaction gas.

After calcination at 500 °C, the activities of CN-2 catalysts decrease significantly (Table 5), which are in agreement with the results of Epling and Hoflund [9]. They reported that 5 wt% Pd/ZrO_2 calcined at 110 and 280 °C catalyze the oxidation reaction more effectively than those calcined at higher temperature, and

Table 4
Catalytic activities of CN-1 catalysts for CH_4 combustion

ZrO_2 content (%)	Temperature (°C)			
	$T_{10\%}$	$T_{20\%}$	$T_{90\%}$	$T_{100\%}$
0	280–290	300	360	380
0[a]	270–280	290–300	350–360	380
2	280	290–300	350–360	380
2[a]	250–260	280–290	350	370
5	280–290	300	350–360	370
5[a]	270	280–290	340–350	360
10	280	290–300	350–360	370
10[a]	260	270–280	340–350	360
20	280–290	300–310	350–360	380

[a] Second test cycle.

supposed "the surface hydroxyl groups are believed to participate in the reaction" [9]. After reduction in H_2, the activities on CN-3 catalysts decrease further. Burch et al. [28] have demonstrated that the metallic Pd is not the active for methane combustion. However, it is not clear until now that whether metallic Pd supported, PdO or a mixed phase Pd^0/PdOx is more active for methane oxidation. Grunwaldt et al. [16] have reported that the presence of more metallic Pd on pre-reduction Pd/ZrO_2 in the reaction is beneficial for the CH_4 combustion.

Yang et al. [14] have suggested that Pd/ZrO_2 have higher activity for catalytic combustion than Pd/Al_2O_3 due to the higher oxygen mobility of ZrO_2 than that of Al_2O_3. Ciuparu et al. [15] have also reported that the rapid exchange of oxygen between ZrO_2 and oxygen in reaction gas can maintain PdO phase available for the methane combustion.

CO pulse reaction results show that the presence of ZrO_2 on Al_2O_3 can enhance the ability of providing active oxygen species. However, this enhancement cannot accelerate the activity of $Pd/ZrO_2/Al_2O_3$ for methane combustion as the expectation. It implies that the lattice oxygen is not the major

Table 5
Catalytic activities of CN-2 catalysts for CH_4 combustion

ZrO_2 content (%)	Temperature (°C)			
	$T_{10\%}$	$T_{20\%}$	$T_{90\%}$	$T_{100\%}$
0	300–310	320	390	410–420
2	310–320	330	400	420–430
5	300	320	390–400	420
10	300	310–320	390	410–420
20	310	320–330	400	420–430

Table 6
Catalytic activities of CN-3 catalysts for CH_4 combustion

ZrO_2 content (%)	Temperature (°C)			
	$T_{10\%}$	$T_{20\%}$	$T_{90\%}$	$T_{100\%}$
0	320–330	340	400–410	430
2	310–320	330–340	410	440
5	310	320–330	390–400	420
10	310	320–330	400–410	430
20	310	330	410–420	440–450

factor for CH_4 oxidation under the great excess oxygen condition, which is not in complete agreement with those presented in other studies. Maybe, it was due to differences in reaction condition and/or catalysts. The effects of properties of ZrO_2/Al_2O_3 on Pd state and the role of lattice oxygen in CH_4 catalytic combustion still need to be investigated further.

4. Conclusions

For ZrO_2/Al_2O_3 composite oxides prepared, ZrO_2 is highly dispersed on the surface of Al_2O_3 when ZrO_2 content is lower than 10 wt%, and tetragonal crystallites are formed beyond this value. The presence of a small amount ZrO_2 can increase surface area and pore volume of composite supports. The strong interaction between ZrO_2 and Al_2O_3 results in the increase of acidity of the support.

The CO–TPD results show that the presence of ZrO_2 enhances the adsorption capacity of CO and the activation of C=O bond leads to the increase of catalytic activity of catalyst for CO oxidation.

The ability of providing active oxygen species increases following the presence of ZrO_2 in Al_2O_3, and the temperature of lattice oxygen activated decreases with increasing ZrO_2 content. However, this cannot promote the activity of Pd/ZrO_2/Al_2O_3 for methane combustion. It implies that the lattice oxygen is not the major factor for methane oxidation under the great excess oxygen condition.

0.2% Pd/ZrO_2/Al_2O_3 (CN-1) catalysts as-prepared show the high activity for CH_4 combustion, and the activities can be further enhanced following the repeat run. The increase of treatment temperature and pre-reduction can decrease the activity of catalyst for CH_4 combustion.

Acknowledgements

This study was supported financially by National Basic Research Program of China (2004CB719500), National Natural Science Foundation of China (20601008), Shanghai Rising-Star Program (05QMX1415) and Nanotechnology Developing Fund (0452nm005) by The Commission of Science and Technology of Shanghai Municipality.

References

[1] M.F.M. Zwinkels, S.G. Jaras, P.G. Menon, Catal. Rev. Sci. Eng. 35 (1993) 319.
[2] T.V. Choudhary, S. Banerjee, V.R. Choudhary, Appl. Catal. A 234 (2002) 1.
[3] M. Faticanti, N. Cioffi, S. De Rossi, N. Ditaranto, P. Porta, L. Sabbatini, T. Bleve-Zacheo, Appl. Catal. B 60 (1–2) (2005) 73.
[4] Y. Ozawa, Y. Tochihara, A. Watanabe, M. Nagai, S. Omi, Appl. Catal. A 258 (2) (2004) 261.
[5] R.J.H. Grisel, J.J. Slyconish, B.E. Nieuwenhuys, Top. Catal. 16 (1–4) (2001) 425.
[6] W.J. Shen, M. Okumura, Y. Matsumura, M. Haruta, Appl. Catal. A 213 (2) (2001) 225.
[7] P. Bera, K.C. Patil, V. Jayaram, G.N. Subbanna, M.S. Hegde, J. Catal. 196 (2) (2000) 293.
[8] Y. Deng, T.G. Nevell, Catal. Today 47 (1999) 279.
[9] W.S. Epling, G.B. Hoflund, J. Catal. 182 (1999) 5.
[10] K. Fujimoto, F.H. Riberio, M. Avalos-Borja, E. Iglesia, J. Catal. 179 (1998) 431.
[11] K. Sekizawa, H. Widjaja, S. Maeda, Y. Ozawa, K. Eguchi, Catal. Today 59 (2000) 69.
[12] K. Nomura, K. Noro, Y. Nakamura, H. Yoshida, A. Satsuma, T. Hattori, Catal. Lett. 58 (1999) 127.
[13] C.A. Müller, M. Maciejewski, R.A. Koeppel, A. Baiker, Catal. Today 47 (1999) 245.
[14] S. Yang, A. Maroto-Valiente, M. Benito-Gonzalez, I. Rodriguez-Ramos, A. Guerrero-Ruiz, Appl. Catal. B 28 (2000) 223.
[15] D. Ciuparu, E. Altman, L. Pfefferle, J. Catal. 203 (2001) 64.
[16] J. Grunwaldt, M. Maciejewski, A. Baiker, Phys. Chem. Chem. Phys. 5 (2003) 1481.
[17] M.M.V.M. Souza, M. Schmal, Appl. Catal. A 281 (1–2) (2005) 19.
[18] Z. Dang, B.G. Anderson, Y. Amenomiya, B.A. Morrov, J. Phys. Chem. 99 (1995) 14437.
[19] T. Klimova, M. Rojas, P. Castillo, R. Cuevas, J. Ramirez, Micropor. Mesopor. Mater. 20 (4–6) (1998) 293.
[20] S. Damyanova, P. Grange, B. Delmon, J. Catal. 168 (1997) 421.
[21] R. Lòez Cordero, F.J. Gil Llambias, A. Lòez Agudo, Appl. Catal. 74 (1991) 125.
[22] D. Duprez, Stud. Surf. Sci. Catal. 112 (1997) 13.
[23] M. Labaki, S. Siffert, J.F. Lamonier, E.A. Zhilinskaya, A. Aboukaïs, Appl. Catal. B 43 (2003) 261.
[24] Q. Zhao, X. Wang, T. Cai, Appl. Surf. Sci. 225 (2004) 7.
[25] J. Matta, J.F. Lamonier, E.A. Aad, E.A. Zhilinskaya, A. Aboukaïs, Phys. Chem. Chem. Phys. 1 (1999) 4975.
[26] J. Zhu, J. Gan, H.J.M. Ommen, L. Bouwmeester, Leffert J. Catal. 233 (2005) 434.
[27] T.R. Baldwin, R. Burch, Catal. Lett. 6 (1990) 131.
[28] R. Burch, F.J. Urbano, Appl. Catal. A 124 (1995) 121.